Supporting information

Assessment of xanthan gum and xanthan-g-silica derivatives as chemical flooding agents and rock wettability modifiers

Ahmed Ashraf Soliman[1,*], Abdelaziz Nasr El-hoshoudy[1,2], and Attia Mahmoud Attia[1,3]

[1]Department of Petroleum Engineering, Faculty of Engineering, British University in Egypt (BUE), Elshorouk city, Cairo 11837, Egypt
[2]Department of Production, Egyptian Petroleum Research Institute, Naser City, Cairo 11727, Egypt
[3]Faculty of Energy and Environmental Engineering, British University in Egypt (BUE), Elshorouk city, Cairo 11837, Egypt

Table S1. Ionic composition of saline solutions used in rheological and flooding tests

Ions	Ions concentration, g/L			
Na^{+}-ion(NaCl)	1.533	4.380	6.569	8.759
K^{+}-ion (KCl)	0.010	0.030	0.044	0.059
Mg^{+2}-ion ($MgCl_2.6H_2O$)	0.021	0.059	0.089	0.118
Ca^{+2}-ion ($CaCl_2.2H_2O$)	0.062	0.176	0.264	0.352
CL^{-}-ion	1.625	4.644	6.966	9.288
HCO_3^{-}-ion ($NaHCO_3$)	0.012	0.036	0.053	0.071
SO_4^{-2}-ion (Na_2SO_4)	0.237	0.677	1.015	1.353
Total dissolved solids (TDS)	**3.50**	**10.00**	**15.00**	**20.00**

Brine solutions prepared from double distilled water and analytical purified chemicals then filtrated with 3.0 μm nucleopore membrane to eliminate suspended constituents and evacuated for about 4 hours prior to usage.

Table S2. Physical properties and dimensions of core samples

# Core	L	r	A	V_B	V_P	ϕ	Δp	K
	(cm)	*(cm)*	*(cm^2)*	*(cc)*	*(cc)*	*(%)*	*(psi)*	*(md)*
1P	5.486	1.892	11.246	61.695	17.275	28.001	1.00	538.0
2P	4.651	1.891	11.243	52.291	14.744	28.196	0.45	583.0
3P	5.604	1.903	11.387	63.815	18.122	28.398	0.37	565.0
4P	5.329	1.941	11.844	63.114	18.177	28.800	0.37	599.0
5P	5.327	1.896	11.298	60.184	15.527	25.799	0.45	522.0
1R	5.075	1.892	11.253	57.110	14.847	25.997	0.36	347.0
2R	4.795	1.893	11.268	54.031	14.371	26.598	0.69	433.0
1F	5.093	1.898	11.323	57.669	16.027	27.791	0.17	396.0
2F	5.341	1.870	10.987	58.683	15.34	26.140	0.31	688.0
1kL	5.197	1.943	11.860	61.638	16.312	26.464	0.32	551.0
Maximum	5.604	1.943	11.860	63.815	18.177	28.800	1	688.000
Minimum	4.651	1.870	10.987	52.291	14.371	25.799	0.17	347.000
Average	5.190	1.902	11.371	59.023	16.074	27.218	0.45	522.200

Table S3. Pressure differential profiles of the three displacing fluids (XG, XG/SiO_2, and XG-g-silica composite)

Parameters	XG-polymer	XG/SiO_2	XG-g-silica
Core# ID	1R	3P	2R
Average pore radius (r), µm	1.892	1.903	1.893
Flooding Temperature, ºC	25	25	25
Shear rate, s^{-1}	10.22	10.22	10.22
Brine viscosity at flooding conditions, mPa.s	1.040	1.040	1.040
viscosity of the polymer solution, mPa.s	75.000	85.000	95.000
Oil viscosity, mPa.s	8.960	8.960	8.960
Brine permeability (K_w), mD	560.550	560.550	560.550
Water-polymer Permeability (K_{wp}), mD	104.100	160.000	200.500
Oil Permeability (K_o), mD	14.100	21.100	25.000
$(\Delta P)_P$,psi	6.250	7.980	9.650
$(\Delta P)_{W\ (Before\ Polymer)}$,psi	0.273	0.273	0.273
$(\Delta P)_{W\ (After\ Polymer)}$,psi	3.410	3.740	4.450
R_f	22.894	29.231	35.348
R_{ff}	12.491	13.700	16.300
ξ	0.886	0.914	0.951
Mobility ratio (M)	0.882	0.799	0.756

The ability of fluids to flow across the porous media evaluated through the resistance and residual resistance factors (R_f & R_{ff}) respectively. The pressure differential profiles follow this arrangement XG-g-silica >XG/SiO_2>XG-polymer, this may resort to increasing of intramolecular associations between polymer chains and silanol groups which increase hydrodynamic volume and the solution viscosity. Moreover, hydrophilic nanosilica particles adsorbed on the porous rock surface and form a hydrophilic network structure which increases the permeability resistance. Although XG-g-silica & XG/SiO_2 greatly increase permeability reduction, they could navigate easily through rock throats without producing plugging or internal filterable lump. Moreover, the mobility ratio (M) is less than unity, which reveals higher sweeping efficiency through porous media and consequently higher oil recovery.

Fig. S1, Fourier Transformation spectroscopy of SiO_2, and XG-g-silica composite

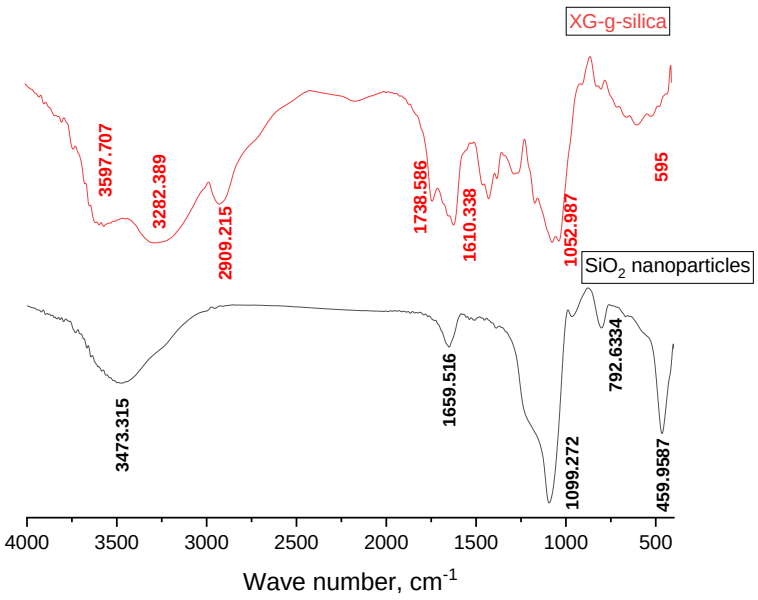

Characteristic bands of **xanthan gum** involving strong band at 3597-3282 ($\upsilon_{(O–H)}$ axial deformation; 2909 ($\upsilon_{(C–H)}$ stretching vibrations of (C-H) group in $-CH_3$ & $-CH_2-$ groups; 1738 ($\upsilon_{(C=O)}$ stretching vibration in ester); 1610 ($\upsilon_{(C-O)}$ axial deformation of enols in ether; in addition to vibrations at 1052 & 594 cm^{-1} related to stretching and winding vibration of (Si-O-Si) structure in the silica network, respectively.

Fig. S2, ^{1}H NMR spectra (a) Xanthan gum and (b) XG-g-silica composite respectively

a)

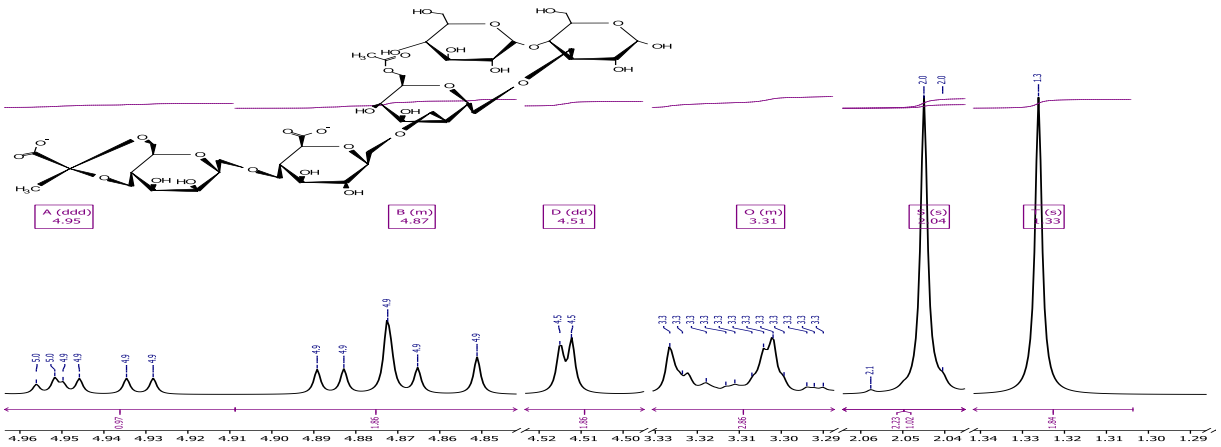

b)

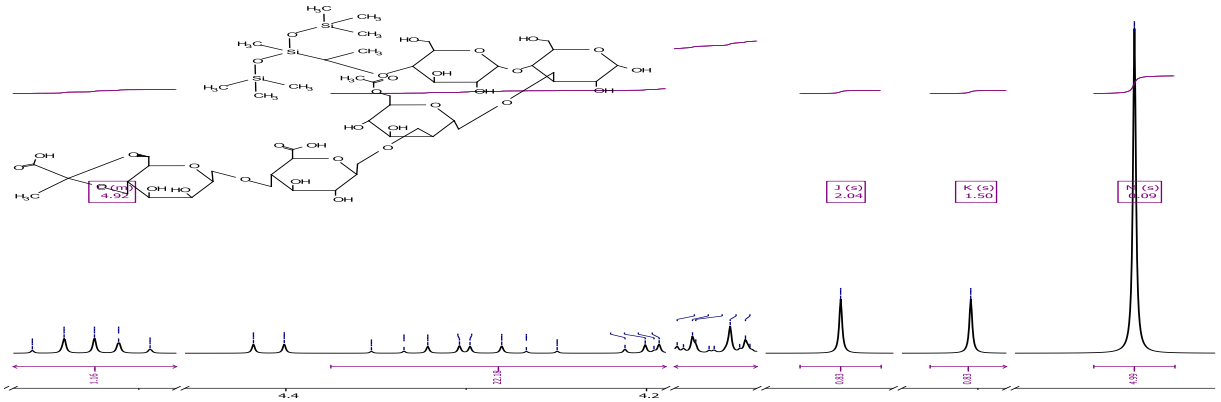

Xanthan gum displays chemical shifts at δ (ppm) = 1.33 (s, 3H, terminal (-CH_3) group of pyruvate); 2.04 (s, 3H, terminal -CH_3 group of acetyl group in α-D-mannose); bands at 3.31 (m,1H, OH) related to pendant (-OH) groups in α, β-D-mannose; chemical shifts at δ (ppm) = 3.56- 4.95 correspond to several (m,s,dd,t,ddd) peaks of (-OH & -CH_2) groups of anhydro glucose units in xanthan structure.

The ^{1}H-NMR spectrum of XG-g-silica composite exhibit all chemical shifts of xanthan gum in addition to chemical shift at δ (ppm)=0.09 (s, 18H, 2[-Si(CH_3)$_3$], which indicates polymerization of methylbis(trimethylsilyloxy) vinylsilane with xanthan gum.

Fig. S3, Thermal gravimetric analysis of SiO_2, Xanthan gum, and XG-g-silica composite

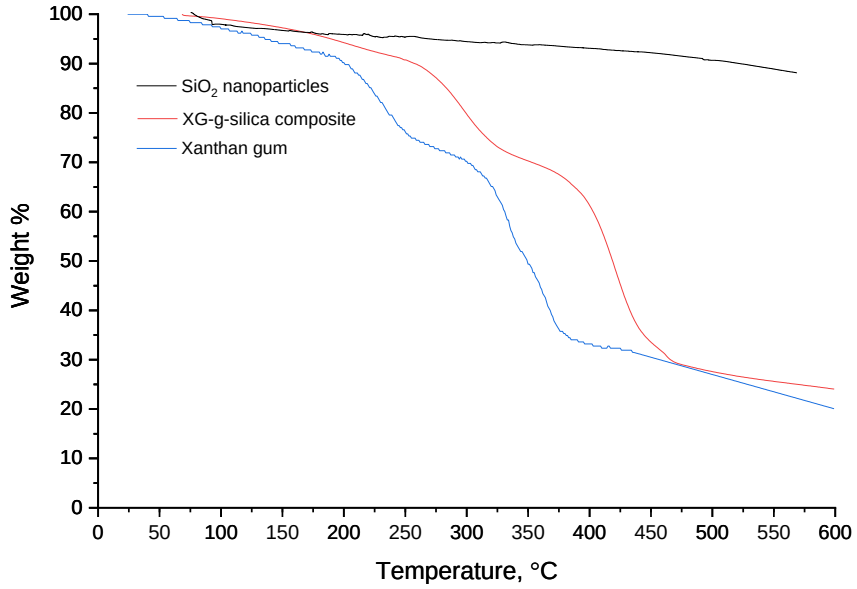

SiO_2 nanoparticles exhibit weight loss is nearly negligible since the material prepared by calcination at 550 °C for 4 hours. **Xanthan gum** exhibit weight loss of 3.7% at 100 °C due to adsorbed water loss, and incrementally increase with heat flow increasing up to 300 °C due to intramolecular and intermolecular moisture evaporation. Approximately 30% of the weight loss occurs between 100 and 300 °C and reach 69% weight loss at 450°C. Beyond 450°C, the residual mass reaches 24 wt%. This may revert to thermal decomposition of the xanthan gum rings and hydrocarbon structure. **XG-g-silica composite** exhibit the same weight loss regimes as xanthan gum, but beyond 450°C, the total mass residue was 31% only. This thermal stability enhancement resort to grafting of the silica into polymer architecture, which forms dense and compacted structure.

Fig. S4, TEM photographing of (a) SiO_2, and (b) XG-g-silica composite

a)

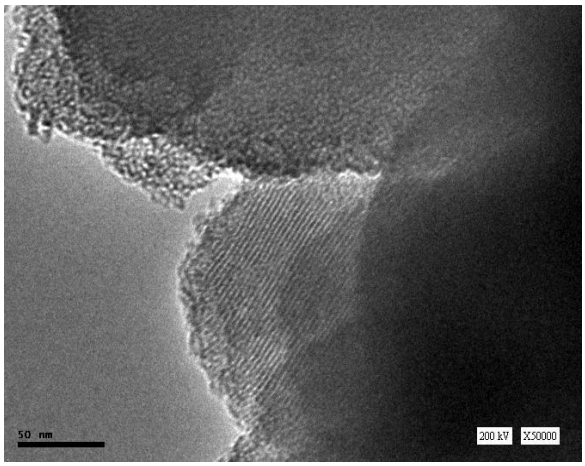

b)

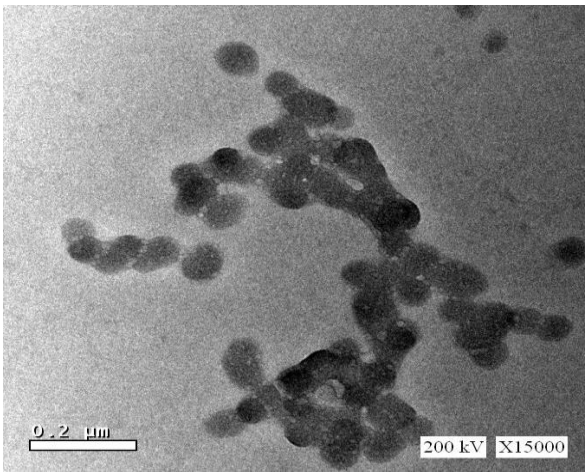

SiO_2 display ordered slightly amorphized structure. XG-g-silica composite appeared as irregularly distributed dark and light rounded ball-shaped zones which indicate that silanol moieties precipitated as a dark core surrounded with light xanthan gum shell.

Scheme S1, Formation reaction of XG-g-silica composite